



UvA-DARE (Digital Academic Repository)

Transient and variable radio sources in the LOFAR sky: an architecture for a detection framework

Scheers, L.H.A.

Publication date
2011

[Link to publication](#)

Citation for published version (APA):

Scheers, L. H. A. (2011). *Transient and variable radio sources in the LOFAR sky: an architecture for a detection framework*. [Thesis, fully internal, Universiteit van Amsterdam].

General rights

It is not permitted to download or to forward/distribute the text or part of it without the consent of the author(s) and/or copyright holder(s), other than for strictly personal, individual use, unless the work is under an open content license (like Creative Commons).

Disclaimer/Complaints regulations

If you believe that digital publication of certain material infringes any of your rights or (privacy) interests, please let the Library know, stating your reasons. In case of a legitimate complaint, the Library will make the material inaccessible and/or remove it from the website. Please Ask the Library: <https://uba.uva.nl/en/contact>, or a letter to: Library of the University of Amsterdam, Secretariat, P.O. Box 19185, 1000 GD Amsterdam, The Netherlands. You will be contacted as soon as possible.

Cross-Matching Multiple Radio Catalogues

Abstract

The calibration of LOFAR relies on flux measurements of strong radio sources with accurate positions and well-known spectra, i.e., the calibrator sources. Since the source properties are not well determined in the relatively unexplored frequency range of LOFAR (30–240 MHz), we have to interpolate and/or extrapolate the existing spectra of calibrator sources to the LOFAR frequencies. Therefore, we quantitatively cross-correlate sources from multiple catalogues to collect the spectral information in calibrator source lists.

The aim is to construct high-quality source lists with spectral information at three frequencies, 74, 325 and 1400 MHz, of which the lowest frequency falls in the LOFAR Low Band.

We quantify the likelihood of true and false associations between catalogues, and develop a criterion for accepting associations; we apply this method to cross-identify sources in the VLSS, WENSS, and NVSS catalogues.

We present a high-quality source list of nearly 2800 VLSS sources in the declination strip of $44^\circ \leq \delta \leq 64^\circ$, that are brighter than 1 Jy ($10\sigma_{\text{rms}}$) at 74 MHz and have unique counterparts in the WENSS and NVSS catalogues at 325 and 1400 MHz, respectively. Nearly 90% of the sources show a spectrum that turns over towards lower frequencies, and 27 sources display a peaked spectrum.

The association method can also be used in the search for transient sources, when source detections in repeated scans of the same areas of sky need to be compared with potential counterparts that are catalogued as previously detected; here also, a strict and quantitative criterion must be used to decide whether to accept that a new measurement is of the same source as previous ones.

4.1 Introduction

Finding which source in one catalogue is genuinely associated to which source in another catalogue is a classical problem in astronomy. Conventional procedures involve the angular distance between sources as a qualification for the association. Prior knowledge about the astrometry and resolution of the catalogues then determines an applicable threshold to be set. However, the flexibility of LOFAR allows many possible configurations of observational modes, resulting in a wide range of sensitivities and resolutions (e.g., De Vos et al., 2009; Nijboer & Pandey-Pommier, 2009). The large number of measurements of sources expected to be detected by LOFAR (see Chapter 2) will consequently produce large catalogues. Cross-matching sources between the LOFAR catalogue and other catalogues, will find either no, one or more possible counterparts. This asks for association procedures that are quantitative and by which reliable decisions can be made to accept or reject an association.

One part in the calibration process of LOFAR depends on flux measurements of strong radio sources, of which the positions and fluxes at given frequencies need to be known accurately beforehand. The large fields of view of LOFAR require many such calibrator sources. However, the low-frequency domain of LOFAR is relatively unexplored, so that the spectral behaviour of radio sources is not well covered. Therefore, we start by building an initial list of calibrator sources by quantitatively cross-correlating existing major catalogues. Sources with matching positions that are classified as a genuine association are added to this list. Calibrator fluxes at any LOFAR frequency are then given by the interpolations and/or extrapolations from this list. The list is, however, not static, but will evolve over time as new measurements made by LOFAR are added, resulting in more (calibrator) sources and a denser sky and frequency coverage. This list of sources represents the so-called Global Sky Model (GSM).

Similar source lists need to be created for the Transients Key Project. Since the lists will contain *all* sources detected by LOFAR, it is more appropriate to term them "LOFAR catalogue". The Transients Key Project searches for new sources to appear or known sources to change in the LOFAR sky. One way of doing that is by comparing new measurements of sources with the archived measurements in the LOFAR catalogue. This again requires source associations with quantifiable fidelity. Because of the large data volumes and high cadence of LOFAR measurements (see Chapter 2), we embedded the association procedures in the automated software pipeline of the TKP (e.g., Chapter 3 of this thesis; Swinbank et al., 2007; Swinbank, 2010).

Several methods exist that produce source lists by cross-identifying different catalogues, e.g., cross-identifications of radio sources with radio and optical catalogues (Helmboldt et al., 2008; Kimball & Ivezić, 2008), and

	VLSS	WENSS		NVSS
		main	polar	
Sky Coverage	$\delta \geq -30^\circ$	$28^\circ \leq \delta \leq 76^\circ$	$\delta \geq 72^\circ$	$\delta \geq -40^\circ$
Frequency [MHz]	73.8	325	352	1400
# Sources	68,311	211,225	18,185	1,773,484
Resolution	80''	$54'' \times 54'' \csc \delta$		45''
Sensitivity [mJy]	100	3.6		0.45
Astrometry [arcsec]	3'' – 10''	1.5'' – 5''		1'' – 7''
Source Density [deg ⁻²]	2	22		55

Table 4.1: Characteristics of the major radio catalogues, VLSS, WENSS and NVSS.

of X-ray sources with optical and near-infrared catalogues (Pierre et al., 2007; Rutledge et al., 2000; Haakonsen & Rutledge, 2009). We adopt the quantitative cross-identification analysis of Rutledge et al. (2000) to produce high-quality source lists.

To have source lists with overlap with the LOFAR frequencies, we used the sources that were detected in three major radio surveys¹, at 74 MHz the VLA Low-Frequency Sky Survey (VLSS), at 325 or 352 MHz the Westerbork Northern Sky Survey (WENSS) and at 1.4 GHz the NRAO VLA Sky Survey (NVSS). Table 4.1 shows the main characteristics of the radio catalogues used in our samples.

The VLSS (Cohen et al., 2007) surveyed the sky north of $\delta = -30^\circ$ at 73.8 MHz. The resolution is 80'' and the limiting point source flux density is 0.7 Jy, with typical rms noise levels at about 0.1 Jy. Positional uncertainties are of the order of 3'' – 10''. The latest version (2007-06-26) contains 68,311 sources.

The WENSS catalogue (Rengelink et al., 1997) contains 229,420 sources of which 18,186 are from the polar catalogue ($\delta \geq 72^\circ$) at 352 MHz and the rest from the main catalogue ($28^\circ \leq \delta \leq 76^\circ$) at 325 MHz. Ten sources in the catalogue are without flux values and they were not taken into account. The resolution of the survey is $54'' \times 54'' \csc \delta$, and for both parts the limiting flux density is 18 mJy (5σ). The positional accuracy depends on the ratio of flux density and local rms and is about 5.5'' for the faint and 1.5'' for the stronger sources. The positional uncertainties of the sources were calculated using Eq. 8 in Rengelink et al. (1997).

The NVSS catalogue (Condon et al., 1998) covers the sky north of declination -40° at 1.4 GHz. It contains 1,773,484 sources with a limiting flux

¹We extracted the catalogues from the VizieR Astronomical Server at <http://cdsarc.u-strasbg.fr/viz-bin/VizieR> and loaded them into the database that is implemented in the Transients Key Project software pipeline. The source code of the latter is stored in the password-protected `svn` repository, available at <http://svn.transientskp.org/code>.

density of about 2.5 mJy (5σ). The resolution is $45''$ and rms positional uncertainties vary from less than $1''$ for sources stronger than 15 mJy to $7''$ for the faintest ones.

The organisation of this Chapter is as follows. Section 4.2 describes the three association parameters, which are the properties of every source association pair. In Section 4.3 we apply the method of Rutledge et al. (2000) to cross-correlate the WENSS and NVSS catalogues, resulting in a high-quality list of reliable WENSS–NVSS associations. In Section 4.4 we include the VLSS catalogue as well, to construct a high-quality source list of nearly 2,800 sources with flux measurements at 74, 352 and 1400 MHz. We discuss the results in the last section.

4.2 Association Parameters

We repeat the three parameters that are defined for every source association pair (see Chapter 3): The first parameter is the angular distance between the two sources

$$\theta = 2 \arcsin\left(\frac{1}{2}\sqrt{(\Delta x)^2 + (\Delta y)^2 + (\Delta z)^2}\right), \quad (4.1)$$

where $\Delta x, \Delta y, \Delta z$ are the Cartesian coordinate differences (on a unit sphere) of the sources. The second parameter is the weighted dimensionless distance

$$r = \sqrt{\frac{(\Delta\alpha)^2}{\sigma_{\Delta\alpha}^2} + \frac{(\Delta\delta)^2}{\sigma_{\Delta\delta}^2}}, \quad (4.2)$$

with $\Delta\alpha = \alpha_i \cos \delta_i - \alpha_j \cos \delta_j$ the measured right ascension difference corrected for declination, and $\Delta\delta$ the measured declination difference. Both are weighted by their positional errors summed in quadrature. A third parameter is based on the ratio of the probability of finding a true association at r and an association by chance due to a background source that happens to be at r from the source. This is the likelihood ratio

$$LR = \frac{\exp(-r^2/2)}{2\pi\sigma_{\Delta\alpha}\sigma_{\Delta\delta}n_L(\nu, S_{\text{lim}})}, \quad (4.3)$$

where n_L is the local source density, as function of frequency and flux. Because we only associate sources by positional matches, we consider it as constant here and adopt the average NVSS source density. A more convenient way of expressing the likelihood is in logarithmic form: $\Lambda \equiv \log LR$.

4.3 Reliability of WENSS–NVSS Associations

4.3.1 Source Selection Criteria

From the WENSS catalogue we selected only point sources that were classified as type ‘S’ sources (meaning they could be fitted with a single Gaussian component; Rengelink et al., 1997), and were not flagged as having caused fitting problems. A further selection was set by the declination. We included sources falling in the declination strip of $44^\circ \leq \delta \leq 64^\circ$, as they are all from the main catalogue part of the WENSS catalogue at the single frequency of 325 MHz (see Table 4.1). This sky coverage is identical to the Zenith Monitor mode of LOFAR (see Chapter 2). We join this set of WENSS sources with the NVSS catalogue to search for cross-identifications.

We adopt the quantitative cross-identification method of Rutledge et al. (2000) and apply it as follows. We define a *Source Field* of radius $90''$ around every WENSS source. For every WENSS source, we consider all NVSS sources falling within an angular distance of $90''$ as an association candidate and we calculate its likelihood ratio, Λ . These candidates, in a *Source Field*, include true and false associations. At the same time, we positionally offset every WENSS source to eight locations, surrounding the original WENSS source to mimic the local source density. We define eight *Background Fields* centred at the offset locations, all with identical radii as the *Source Field*. The non-overlapping *Background Fields* surround the *Source Field* on a rectangular 3×3 grid with spacings of $180''$ to the neighbouring *Fields*. A copy of the WENSS source is then placed at the centre of every *Background Field*. We exclude *Background Fields* that themselves contain a WENSS source, since we assume that *Background Fields* do not contain an NVSS source that could be associated with a WENSS source. These offset sources in the *Background Fields* were then processed analo-

	N_{assoc}	Source Field	BG Field	All BG Fields
N_{field}		74,314	71,730	573,837
	0	6,397	67,330	538,637
	1	64,504	4,235	33,880
	2	3,330	158	1,263
	3	82	7	54
	4	1	0	3
	> 0	71,414	4,573	36,580

Table 4.2: The number of *Source Fields* and *Background Fields*, N_{field} , that were used for the WENSS–NVSS associations at $44^\circ \leq \delta \leq 64^\circ$. 20,675 *Background Fields* contained a WENSS source themselves and were excluded. N_{assoc} is the number of associations that a unique source has with an NVSS source. It can be seen that 6,397 WENSS sources did not have an NVSS source within $90''$.

gously to the original WENSS sources. NVSS counterparts found for the offset sources are regarded as purely false. Statistical analysis of the number counts then determines the likelihood regime in which associations are considered as genuine. We derive the probability for the association being unique.

Table 4.2 shows the total number of Fields used in the sample and the number counts for NVSS associations made in Source and Background Fields.

4.3.2 Parameter Evaluation

We divide the Source and Background Fields into N_{rings} rings of equal areas: we draw N_{rings} concentric circles around the Field centre, with the radii of the circles defined as $\rho_i^2 = i \rho_1^2$, $i = 1, 2, \dots, N_{\text{rings}}$, with $\rho_1 = 10''$. If we then count the number of NVSS sources falling in circular areas between two adjacent circles, ρ_i and ρ_{i+1} , we would expect the source counts to approach the NVSS source density in the outer rings of the Source Fields. In Background Fields, where we assume associations by chance, we expect the source counts to fluctuate around the NVSS source density. This is shown in Fig. 4.1. Around $i = 20$, i.e. $\rho \approx 45''$, no distinction between a true or false association with an NVSS source can be made anymore. The deficit of NVSS sources in Source Fields in the more outer rings ($i > 28$) is explained by the fact that most NVSS sources in Source Fields are true

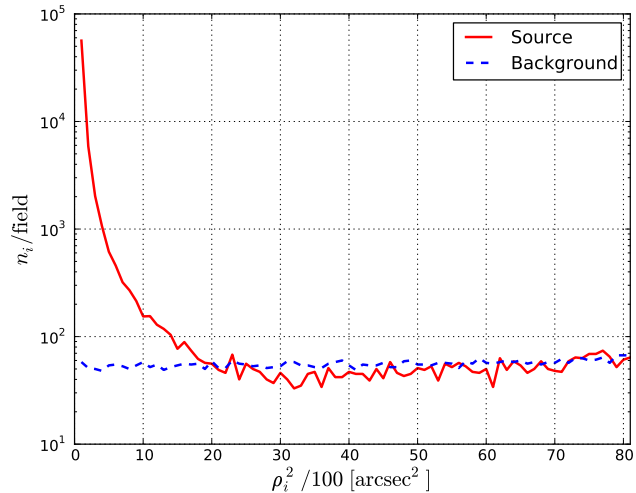


Figure 4.1: Source counts in equal areas of Source (red line) and Background (blue dashed line) Fields. The x -axis shows the ring number i , or $\rho_i^2/100$, and the y -axis the number of NVSS sources falling in ring i . The source counts in the outer rings of the Source Fields approach the average NVSS source density, which is about 52 deg^{-2} .

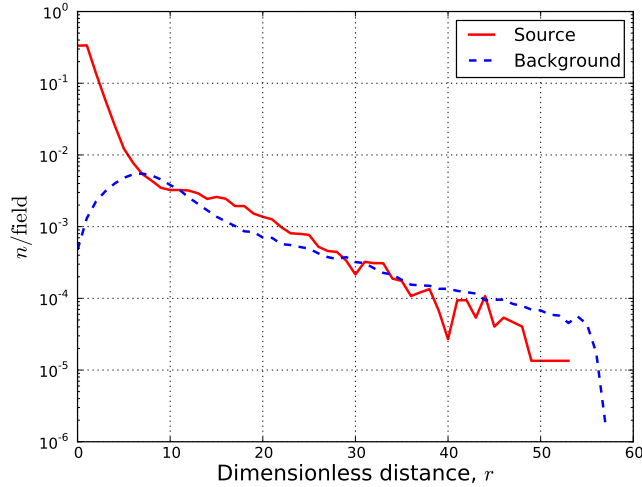


Figure 4.2: The normalised distribution of the dimensionless distance, r , from Eq. 4.2, of the WENSS–NVSS associations in Source (red line) and Background (blue dashed line) Fields. In this plot the binwidth is $dr = 1$.

WENSS counterparts and are more likely to lie in the inner rings, leaving the outer rings more empty.

The positional uncertainties of bright WENSS sources ($S > 10\sigma_{\text{rms}}$) do not have a Gaussian distribution, but are set fixed to $1.5''$ (Rengelink et al., 1997), whereas the faint WENSS sources do have a Gaussian distribution with typical uncertainties of $5.5''$. Therefore, the normalised distribution of the dimensionless distance, r , of the source association pairs does not strictly follow a Rayleigh distribution, but is biased towards the bright WENSS–NVSS associations. This can be recognised in Fig. 4.2, where bright WENSS–NVSS (true plus false) associations in the Source Fields tend to have larger r values, and therefore contribute more towards larger r , which explains the excess of associations in the region of $12 \leq r \leq 28$. Furthermore, from the Source Field distribution in Fig. 4.2 it can be seen that the positional uncertainties of the bright WENSS sources were set conservatively. Similar effects are seen in the normalised distribution of the logarithmic likelihood ratio, Λ , which is displayed in Fig. 4.3 for Source and Background Fields.

Following Rutledge et al. (2000) and Haakonsen & Rutledge (2009), and setting $\Lambda_{ij} = \log LR_{ij}$, the reliability of a WENSS–NVSS association pair is given by

$$R_{ij} = R(\Lambda_{ij}) = \frac{N_{\text{true}}(\Lambda_{ij})}{N_{\text{true}}(\Lambda_{ij}) + N_{\text{false}}(\Lambda_{ij})}, \quad (4.4)$$

where $N_{\text{true}}(\Lambda_{ij})$ is the number of true associations for the given Λ_{ij} value in

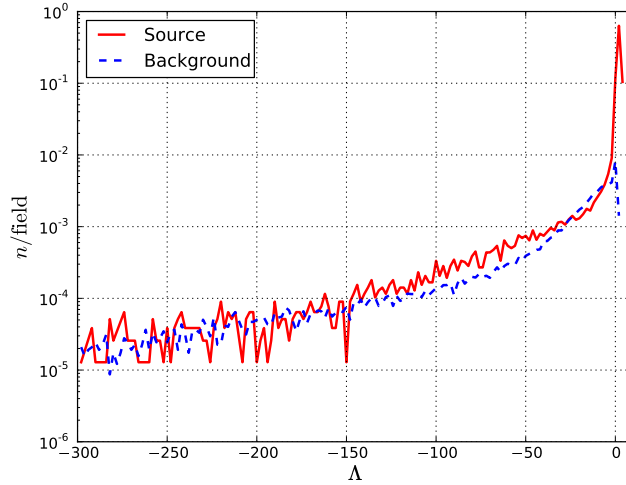


Figure 4.3: The normalised distribution of the logarithmic likelihood ratio, Λ , of the WENSS–NVSS associations in Source (red line) and Background (blue dashed line) Fields. The binwidth is $d\Lambda = 2$.

a Source Field, and $N_{\text{false}}(\Lambda_{ij})$ is the number of false associations in a Source Field for the given Λ_{ij} value. R_{ij} is the probability that a WENSS–NVSS association with likelihood value Λ_{ij} is genuine and not false by a mere coincidental background source. We cannot discriminate *a priori* between true and false counterparts, but we can approximate R by using the total number counts from Source (N_{SF}) and Background (N_{BG}) Fields by setting $N_{\text{SF}}(\Lambda) = N_{\text{true}}(\Lambda) + N_{\text{false}}(\Lambda)$ and $N_{\text{BG}}(\Lambda) = N_{\text{false}}(\Lambda)$. Substituting this into Eq. 4.4 gives

$$R = R(\Lambda) = 1 - \frac{N_{\text{BG}}(\Lambda)}{N_{\text{SF}}(\Lambda)}. \quad (4.5)$$

The reliability is now approximated by the ratio of the normalised number counts for Source and Background Fields. We define a cutoff value in Λ_c below which the reliability is set to zero, $R(\Lambda < \Lambda_c) = 0$. The largest value of Λ where $R(\Lambda) \leq 0$ is set as the cutoff value, which in our sample is at $\Lambda_c = -7.1$. Associations having $\Lambda < \Lambda_c$ are considered unlikely, and are not taken into account. Fig. 4.4 shows the reliability of WENSS–NVSS associations as function of Λ .

At $\Lambda_c \geq 1.9$, i.e. $R \geq 0.99$ we only have two WENSS sources that have two NVSS counterparts, and 58,330 WENSS sources having a single NVSS counterpart. In case of no multiple NVSS associations for a WENSS source, the reliability R is at the same time the probability of the association being unique (Rutledge et al., 2000) and from this a high-quality source list can be constructed.

RA [hh:mm:ss]	Dec [dd:mm:ss]	WENSS	NVSS	θ [arcsec]	r	Λ	$1-R$	α_{W-N}
00:02:35.988	+63:42:04.336	B0000.0+6325	J000236+634204	5.211	3.216	1.925	0.012	0.992±0.030
00:02:35.661	+52:55:49.652	B0000.0+5239	J000235+525548	4.234	2.558	2.746	0.002	0.711±0.036
00:02:36.578	+60:32:20.640	B0000.0+6015	J000237+603220	8.279	1.363	2.595	0.003	1.240±0.108
00:02:36.845	+50:22:20.242	B0000.0+5005	J000236+502220	6.784	0.915	2.631	0.003	-0.295±0.120
00:02:37.149	+61:02:36.146	B0000.0+6045	J000237+610236	10.454	1.447	2.453	0.004	0.431±0.081
00:02:37.753	+45:05:53.649	B0000.0+4449	J000237+450554	10.982	1.682	2.398	0.004	0.405±0.107
00:02:39.244	+63:13:51.781	B0000.0+6257	J000239+631351	2.863	0.552	3.128	0.001	0.763±0.080
00:02:38.936	+44:29:45.094	B0000.0+4413	J000238+442945	8.523	1.067	2.436	0.004	0.661±0.100
00:02:42.722	+46:45:08.974	B0000.1+4628	J000242+464509	10.258	1.854	2.252	0.005	0.002±0.068
00:02:44.435	+48:02:38.557	B0000.1+4745	J000244+480238	2.297	1.159	3.725	0.000	0.828±0.056
00:02:44.177	+45:09:28.466	B0000.1+4452	J000244+450928	4.391	0.861	2.978	0.001	0.073±0.086
00:02:50.393	+51:32:14.595	B0000.2+5115	J000250+513214	1.167	0.726	4.071	0.000	1.005±0.026
00:02:53.543	+62:19:20.436	B0000.3+6202	J000253+621917	6.085	3.068	1.965	0.011	1.345±0.043
00:02:54.689	+54:37:03.124	B0000.3+5420	J000254+543702	3.091	1.916	3.392	0.000	0.803±0.025
00:02:54.648	+52:58:35.308	B0000.3+5241	J000254+525835	3.928	0.612	2.940	0.002	0.768±0.099
00:02:55.225	+53:22:58.622	B0000.3+5306	J000255+532259	2.598	1.528	3.640	0.000	0.843±0.040
00:02:58.704	+44:03:07.187	B0000.4+4346	J000258+440306	5.151	0.703	2.763	0.002	1.050±0.107
00:02:59.960	+44:56:57.856	B0000.4+4440	J000259+445657	3.517	2.033	3.221	0.001	0.580±0.046

Table 4.3: A subset of the WENSS–NVSS association source list. RA and Dec are the weighted averaged coordinates of the associated WENSS (column three) and NVSS (column four) sources. The association parameters θ , r and Λ are given for every pair, as well as $1-R$, the probability of the association being caused by a coincidental background source. The calculated spectral index, α_{W-N} , is given with its 1σ error.

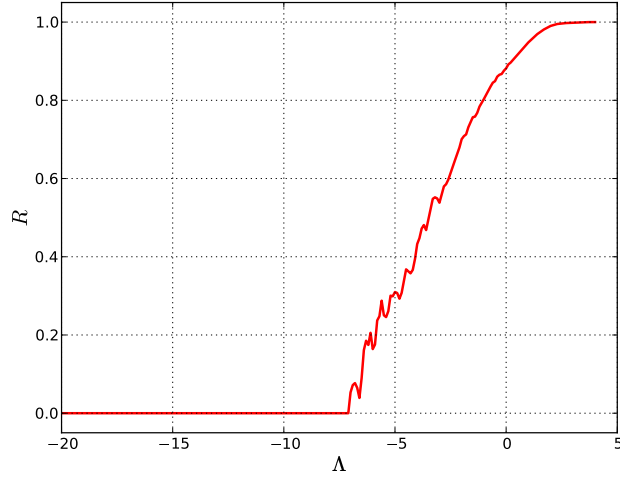


Figure 4.4: The reliability $R(\Lambda)$ for WENSS–NVSS associations having a logarithmic likelihood ratio value of Λ . R is the reliability of an association being genuine and not coincidental, caused by a confusing background source. The bin-width is $d\Lambda = 0.1$. The cutoff is at $\Lambda_c = -7.1$. Below this value, associations are considered as unlikely. Depending on the quality of source lists, other cutoff values are at $\Lambda_c = -3.5$, where $R > 0.5$; $\Lambda_c = 0.2$, where $R > 0.9$; $\Lambda_c = 1.6$, where $R > 0.98$; $\Lambda_c = 1.9$, where $R > 0.99$.

According to a spectrum scaling law of $S_\nu \propto \nu^{-\alpha}$ we can determine the spectral index of the association pair as

$$\alpha_{W-N} = -\frac{\log(S_W/S_N)}{\log(\nu_W/\nu_N)}, \quad (4.6)$$

where S_W , S_N , ν_W and ν_N refer to the WENSS and NVSS fluxes and frequencies, respectively. The error on the spectral index is

$$\sigma_\alpha = c \sqrt{\sigma_{S_W}^2/S_W^2 + \sigma_{S_N}^2/S_N^2}, \quad (4.7)$$

with $c = \log(\nu_N/\nu_W)$ and $\sigma_{S_W}, \sigma_{S_N}$ are the WENSS and NVSS flux errors.

A small selection of the source list of WENSS–NVSS associations with $R \geq 0.99$ is shown in Table 4.3. This list is implemented in the database system used by the Transients Key Project pipeline (Swinbank et al., 2007), and will become available online.

4.4 Cross-Matching Bright VLSS Sources with WENSS and NVSS Sources

We selected all VLSS and NVSS sources in the same declination strip as in Section 4.3.1, at $44^\circ \leq \delta \leq 64^\circ$, and all catalogued WENSS point sources for which a single Gaussian component could be fitted without problems (Rengelink et al., 1997). We accepted only counterparts having a dimensionless distance $r \leq r_{\text{lim}}$, where we set $r_{\text{lim}} = 3.717$. This corresponds to accepting that 0.1% of the genuine source associations will be missed. We further reduced the lists by selecting those sources having $\Lambda \leq \Lambda_c$, with the likelihood ratio cutoff value as determined in Section 4.3.2, $\Lambda_c = -7.1$; additionally we specified a lower limit to the VLSS fluxes, S_{lim} . In the resulting source list we adopted $S_{\text{lim}} = 1 \text{ Jy}$, which corresponds to $10\sigma_{\text{rms}}$ sources.

We processed the cross-correlation as follows. First, we loaded all sources from the NVSS catalogue that satisfied the above-mentioned requirements into a so-called *running* catalogue. This was done to have the catalogue with the highest density as a first reference. Then the WENSS sources were loaded. Positional matches of WENSS sources and sources in the running catalogue (i.e. NVSS sources) obeying $r \leq r_{\text{lim}}$ were considered as an association. The corresponding parameters, θ , r and Λ for every pair were calculated and a weighted average position was maintained in the running catalogue. Lastly, the VLSS sources with $S \geq S_{\text{lim}}$ were loaded and searched

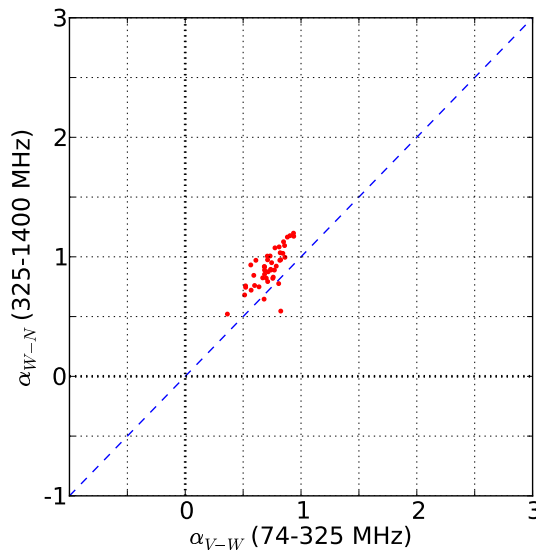


Figure 4.5: Dual spectral indices plot for the 44 sources that have a counterpart in the three catalogues of VLSS, WENSS and NVSS and of which the VLSS source is brighter than 10 Jy.

for counterparts in the running catalogue, which was then updated with the new averaged values for associations found.

Since we explore cross-associations between three catalogues, we calculate the spectral indices between two catalogues that are at adjacent frequencies, analogous to the derivations in Section 4.3.2. Plots of low-frequency spectral indices (α_{V-W} ; between VLSS and WENSS pairs) vs. high-frequency spectral indices (α_{W-N} ; between WENSS and NVSS pairs) give insight into the spectral behaviour of sources. Such dual spectral indices plots are shown in Figs. 4.5, 4.6 and 4.7.

For demonstration purposes, Fig. 4.5 shows the dual spectral indices plot for 44 unique VLSS–WENSS–NVSS associations of which the VLSS source is brighter than 10 Jy ($\sim 100\sigma_{\text{rms}}$). For the final source list, we choose the VLSS lower flux limit at $S_{\text{lim}} = 1$ Jy, to have it at about 10 times the rms noise. Fig. 4.6 shows the corresponding dual spectral indices plot for the 2,791 source associations that meet these requirements. A zoomed-in histogram of the latter source list shows the counts per spectral index cell and is given in Fig. 4.7. Histograms of the two spectral-index distributions are shown in Fig. 4.8, from which it can be seen that the average spectrum turns over towards lower frequencies. Nearly 90% of the sources do show this. The (arithmetic) average spectral indices are $\bar{\alpha}_{V-W} = 0.721$ and $\bar{\alpha}_{W-N} = 0.923$. However, Fig. 4.8 is biased against the larger values of the high-

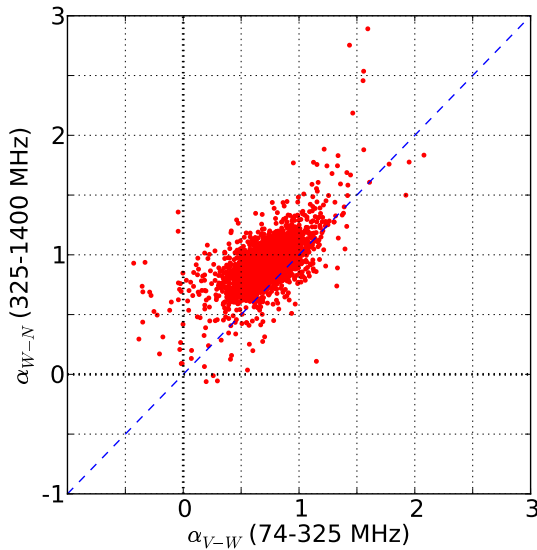


Figure 4.6: Scatter plot of dual spectral indices for the 2,791 sources having a counterpart in all three catalogues of VLSS, WENSS and NVSS and where the VLSS source is brighter than 1 Jy. The fraction of sources having a peaked spectrum resides in the upper left quadrant.

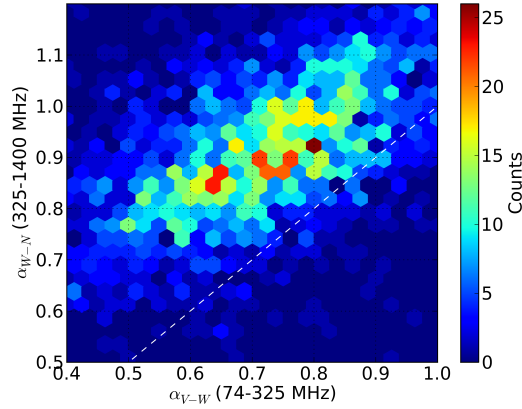


Figure 4.7: Histogram of the dual spectral indices for the 2,791 sources having a counterpart in the three catalogues of VLSS, WENSS and NVSS and where the VLSS source is brighter than 1 Jy.

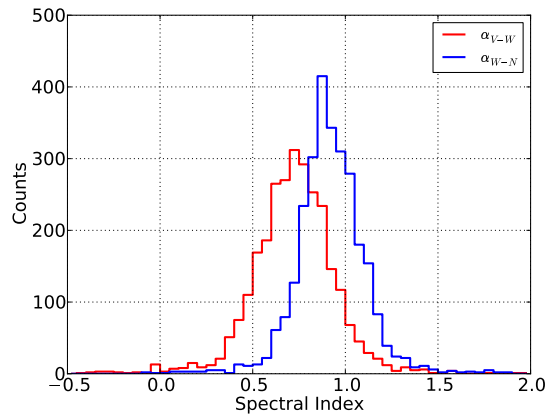


Figure 4.8: Distribution of the low- (α_{V-W}) and high-frequency (α_{W-N}) spectral indices of the 2,791 sources that have counterparts in the three catalogues of VLSS, WENSS and NVSS of which the corresponding VLSS source is brighter than 1 Jy. The arithmetic average spectral indices are $\bar{\alpha}_{V-W} = 0.721$ and $\bar{\alpha}_{W-N} = 0.923$.

4. Cross-Matching Multiple Radio Catalogues

RA [hh:mm:ss]	Dec [dd:mm:ss]	α_{V-W}	α_{W-N}	α_{fit}	χ^2	Catalogue Name	S_r [Jy]	r	Δ
00:00:24.995	44:09:18.251	1.148	0.860	0.925	5.75	VLSS 0000.4+4409 WNH B2357.8+4352 NVSS J000025+440918	1.07±0.14 0.20±0.01 0.06±0.00	0.24 1.04 0.32	3.12 3.96 4.80
00:00:28.869	46:54:42.511	1.422	1.583	1.54	2.42	VLSS 0000.4+4654 WNH B2357.9+4637 NVSS J000028+465443	1.68±0.20 0.20±0.01 0.02±0.00	0.48 1.05 0.59	3.21 3.90 4.37
00:00:49.600	46:00:36.340	0.988	0.760	0.798	3.40	VLSS 0000.8+4600 WNH B2358.2+4543 NVSS J000049+460036	1.12±0.16 0.26±0.01 0.09±0.00	0.63 0.20 0.07	2.82 4.19 4.83
00:01:19.062	47:42:00.738	0.542	0.558	0.555	0.02	VLSS 0001.3+4741 WNH B2358.7+4725 NVSS J000119+474200	1.21±0.16 0.54±0.02 0.24±0.01	1.90 0.22 0.08	2.33 4.19 4.94

Table 4.4: A subset of the source list of the 2,791 VLSS sources brighter than 1 Jy, that have counterparts in both the WENSS and NVSS catalogues. RA and Dec are the weighted average positional coordinates. The calculated two spectral indices for the associations are given by a low-frequency index, α_{V-W} (73.8–325 MHz), and a high-frequency index, α_{W-N} (325–1400 MHz). α_{fit} is the fitted index assuming a straight spectrum, whereas χ^2 is the least squares of the fitted value. The names of the counterparts are given together with the rounded flux values from their original catalogues. r and Δ are the association parameters of the weighted averaged source position and the catalogue counterpart pairs. The reliabilities R are not shown in this table view, since they all are very close to unity.

frequency spectral index: ultra steep spectrum (USS) sources which have a modest WENSS flux will often go undetected in NVSS. If we assume the spectra to be defined by a single power law, given by the VLSS and NVSS flux points, the WENSS fluxes are larger than the expected fluxes from this assumed flux scale by about 14%.

Furthermore, for every source in the list, we fitted a single spectral index, α_{fit} , with the assumption that it has a straight spectrum across the three frequencies on a $\log \nu$ – $\log S_\nu$ scale. The least squares of the fit, χ^2 , is then an indicator for spectra deviating from this assumption, where bent spectra have noticeably larger values than straight spectra. χ^2 values greater than 11.3 correspond to a probability of less than 1% that the spectrum is a single power law.

A small subset of this source list is shown in Table 4.4. It is implemented in the database system that is used by the Transients Key Project pipeline (e.g., Chapter 3 of this thesis; Swinbank et al., 2007; Swinbank, 2010) to be available in real-time during LOFAR observations.

4.5 Discussion and Conclusions

We are able to construct high-quality source lists containing spectral information by evaluating the association parameters (Section 4.2) and applying the quantitative cross-association methods developed by Rutledge et al. (2000). Such source lists serve as an initial Global Sky Model for the LOFAR calibration. The source lists are easily fed into the LOFAR calibration and imaging pipelines, due to the integration of the database system that contains the major catalogues from which the source lists are created.

The likelihood ratio cutoff value, Λ_c , that was determined in Section 4.3.2, is specific to the sample of WENSS–NVSS catalogues. Extensions with the VLSS catalogue were justified, because the local source density, n_L was the same, i.e. the NVSS source density.

The Transients Key Project will maintain a catalogue of all sources detected by LOFAR. The LOFAR catalogue initially comprises the same sources as extracted from the cross-associated catalogues. New measurements of sources are quantitatively associated to the known sources in the LOFAR catalogue, using the same method in order to notice flux changes or detect transient events. The LOFAR catalogue will evolve over time, adding new sources and enhancing the light curve data points of known sources.

In our sample, the majority of the VLSS–WENSS–NVSS cross-associations were unique. If we extend the list of catalogues and are dealing with catalogues of significantly different resolutions, e.g., the optical catalogue of SDSS with $\sim 1''$ resolution, we have to take into account the fact that multiple association candidates will appear in the field of source. In such a field with many possible counterparts, the reliabilities R_{ij} for all the association

pairs will then give the probability for each counterpart being unique or that none can be associated (Rutledge et al., 2000).

From the list of associated sources, we determined the low- and high-frequency spectral indices, which reveal that 90% of the sources have a spectrum that turns over towards lower frequencies, displaying the onset of synchrotron self-absorption. The source list contains 27 sources that have peaked spectra.